# Finite temperature QCD with two flavors of nonperturbatively improved Wilson fermions

V. G. Bornyakov,[1,2,3] M. N. Chernodub,[1,3] H. Ichie,[1] Y. Koma,[4] Y. Mori,[1] Y. Nakamura,[1] M. I. Polikarpov,[3] G. Schierholz,[5,6] A. A. Slavnov,[7] H. Stüben,[8] T. Suzuki,[1] P. V. Uvarov,[3] and A. I. Veselov[3]

(DIK Collaboration)

[1]*Institute for Theoretical Physics, Kanazawa University, Kanazawa 920-1192, Japan*
[2]*Institute for High Energy Physics IHEP, 142284 Protvino, Russia*
[3]*Institute of Theoretical and Experimental Physics ITEP, 117259 Moscow, Russia*
[4]*Max-Planck-Institut für Physik, 80805 München, Germany*
[5]*Deutsches Elektronen-Synchrotron DESY, 22603 Hamburg, Germany*
[6]*John von Neumann-Institut für Computing NIC, Deutsches Elektronen-Synchrotron DESY, 15738 Zeuthen, Germany*
[7]*Steklov Mathematical Institute, 117333 Moscow, Russia*
[8]*Konrad-Zuse-Zentrum für Informationstechnik Berlin ZIB, 14195 Berlin, Germany*
(Received 14 June 2004; published 7 June 2005)

We study QCD with two flavors of nonperturbatively improved Wilson fermions at finite temperature on the $16^3 8$ lattice. We determine the transition temperature at lattice spacing as small as $a \sim 0.12$ fm, and study string breaking below the finite temperature transition. We find that the static potential can be fitted by a two-state ansatz, including a string state and a two-meson state. We investigate the role of Abelian monopoles at finite temperature.

DOI: 10.1103/PhysRevD.71.114504 PACS numbers: 11.15.Ha, 12.38.Aw, 12.38.Gc

## I. INTRODUCTION

Recently, efforts have been made to determine the critical temperature $T_c$ of the finite temperature transition in full QCD with $N_f = 2$ flavors of dynamical quarks. The Bielefeld group employed improved staggered fermions and an improved gauge field action [1]. The CP-PACS Collaboration used improved Wilson fermions with mean field improved clover coefficient and an improved gauge field action [2]. Both groups were able to estimate $T_c$ in the chiral limit, and their values are in good agreement with each other. Still, there are many sources of systematic uncertainties. The main one is that the lattices used so far are rather coarse. In this paper we perform simulations on $N_s^3 N_t = 16^3 8$ lattices at lattice spacings $a$ much smaller than in previous works [1,2]. To further reduce finite cutoff effects, we use nonperturbatively $O(a)$ improved Wilson fermions. A small lattice spacing is particularly helpful in determining the parameters of the static potential.

In the presence of dynamical quarks the flux tube formed between static quark-antiquark pairs is expected to break at large distances. At zero temperature $T$ the search for string breaking, i.e. flattening of the static potential, has not been successful, if the static quarks are created by the Wilson loop. (See e.g. [3]). At finite temperature string breaking has been observed at $T < T_c$, if Polyakov loops are used instead to create the quarks. It is important to know the static potential at finite temperature for phenomenology [4]. In particular, it is needed to compute the dissociation temperatures for heavy quarkonia. We suggest a new ansatz and confront that ansatz with our numerical data.

The dynamics of the QCD vacuum, and color confinement, in particular, becomes more transparent in the maximally Abelian gauge (MAG) [5,6]. In this gauge the relevant degrees of freedom are color electric charges, color magnetic monopoles, ''photons'' and ''gluons'' [7]. There is evidence that the monopoles condense in the low temperature phase of the theory [6,8], causing a dual Meissner effect, which constricts the color electric field into flux tubes, in accord with the dual superconductor picture of confinement [9]. Abelian dominance [10] and the dynamics of monopoles have been studied in detail at zero temperature in quenched [11] and unquenched [12,13] lattice simulations. It turns out that in MAG the string tension is accounted for almost entirely by the monopole part of the Abelian projected gauge field [12,14–16]. Furthermore, in studies of SU(2) gauge theory at nonzero temperature [17] it has been found that at the phase transition the Abelian Polyakov loop shows qualitatively the same behavior as the non-Abelian one. In this paper we extend the investigation of Abelian dominance to full QCD at nonzero temperature.

The paper is organized as follows. In Sec. II we present the details of our simulation. Furthermore, we describe the gauge fixing algorithm and the Abelian projection. Section III is devoted to the determination of the transition temperature, and in Sec. IV our results for the heavy quark potential are presented. In Sec. V we study the monopole density in the vacuum, as well as the action density in the vicinity of the flux tube. We demonstrate that the flux tube disappears at large quark-antiquark separations. Finally, in Sec. VI we conclude. Preliminary results of this work have been reported in [18].

 

## II. SIMULATION DETAILS

We consider $N_f = 2$ flavors of degenerate quarks. We use the Wilson gauge field action and nonperturbatively $O(a)$ improved Wilson fermions [19]

$$S_F = S_F^{(0)} - \frac{i}{2}\kappa g c_{sw} a^5 \sum_s \bar{\psi}(s)\sigma_{\mu\nu}F_{\mu\nu}(s)\psi(s), \qquad (1)$$

where $S_F^{(0)}$ is the original Wilson action, $g$ is the gauge coupling and $F_{\mu\nu}(x)$ is the field strength tensor. The clover coefficient $c_{sw}$ is determined nonperturbatively. This action has been used in simulations of full QCD at zero temperature by the QCDSF and UKQCD Collaborations [20,21], whose results we use to fix the physical scale and the $m_\pi/m_\rho$ ratio. The scale is fixed by the $r_0$. At finite temperature the same action was used before in simulations on $N_t = 4$ and 6 lattices at rather large quark masses and lattice spacings [22].

Nonperturbatively improved $N_f = 2$ Wilson fermions should not be employed below $\beta \equiv 6/g^2 = 5.2$. In fact, $c_{sw}$ is known only for $\beta \geq 5.2$ [23]. The simulations are done on $16^3 8$ lattices at the coupling constant $\beta = 5.2$, and nine different $\kappa$ values. The parameters are listed in Table I. They are also shown in Fig. 1, together with lines of constant $r_0/a$ and constant $m_\pi/m_\rho$ obtained at $T = 0$ [20]. Note that the lines of constant $T$ run parallel to the lines of constant $r_0/a$. To check the finite size effects we have also done simulations on the $24^3 8$ lattice at $\beta = 5.2$, $\kappa = 0.1343$.

The dynamical gauge field configurations are generated on the Hitachi SR8000 at KEK (Tsukuba) and on the MVS 1000M at Joint Supercomputer Center (Moscow), using a Hybrid Monte Carlo, while the analysis is done on the NEC SX5 at RCNP (Osaka) and on the PC-cluster at ITP (Kanazawa). Our present statistics is shown in Table I. The length of the trajectory was chosen to be $\tau = 0.25$.

TABLE I. Parameters and statistics of the simulation, together with the integrated autocorrelation time for the non-Abelian Polyakov loop $\tau_{\mathrm{int},L}$ and for the Polyakov loop susceptibility $\tau_{\mathrm{int},\chi}$. Entries marked with an asterisk are explained in the text.

| | $\beta = 5.2$ | | |
|---|---|---|---|
| $\kappa$ | Traj. | $\tau_{\mathrm{int},L}$ | $\tau_{\mathrm{int},\chi}$ |
| 0.1330 | 7129 | 13(5) | 1.8(2) |
| 0.1335 | 4500 | 38(15) | 5.3(9) |
| 0.1340 | 3000 | 62(27) | 4(1) |
| 0.1343 | 6616 | 190(100) | 17(4) |
| 0.1344 | 8825 | 360(190) | 40(14) |
| 0.1344* | 2450 | | |
| 0.1345 | 6877 | 140(76) | 37(12) |
| 0.1345* | 2200 | | |
| 0.1348 | 5813 | 124(54) | 25(7) |
| 0.1355 | 5650 | 50(16) | 5.3(7) |
| 0.1360 | 3699 | 46(17) | 22(6) |

The more recent runs at $\kappa = 0.1344$ and 0.1345 (marked in Table I with asterisk) use the improved HMC algorithm of Ref. [24] with $\tau = 0.5$. We use a blocked jackknife method to compute the statistical errors. To check the reliability of our error estimates, we also computed the integrated autocorrelation times of the non-Abelian Polyakov loop and of its susceptibility. A bootstrap method was used to compute the errors of the fit parameters. We compute the Polyakov loop

$$L(\vec{s}) = \frac{1}{3}\mathrm{Tr}\prod_{s_4=1}^{N_t} U(s,4), \qquad (2)$$

U$(s, \mu)$ being the link variable, on every trajectory. From that we derive the susceptibility

$$\chi = N_s^3 \sum_{\vec{s}} (\langle L^2(\vec{s})\rangle - \langle L(\vec{s})\rangle^2), \qquad (3)$$

and the integrated autocorrelation time $\tau_{\mathrm{int},L}$, and from (3) we compute the integrated autocorrelation time $\tau_{\mathrm{int},\chi}$. The autocorrelation times are given in Table I in units of trajectories.

As can be seen from Table I, for some of our data sets close to the transition point $\tau_{\mathrm{int},L}$ is large compared to the size of the set. Therefore, a reliable estimate of the statistical error might be questioned in these cases. To check this, we have computed the error by a blocked jackknife method as well as by means of $\tau_{\mathrm{int},L}$ (see, e.g., [25] for details) and found good agreement. This problem is less

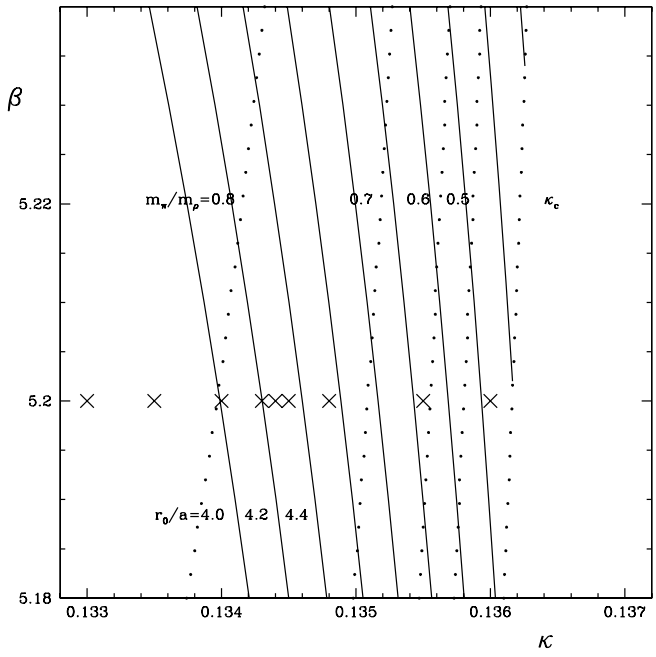


FIG. 1. Lines of constant $r_0/a$ (solid lines) and constant $m_\pi/m_\rho$ (dotted lines) at $T = 0$. Crosses indicate points where simulations are done.

severe for $\tau_{\mathrm{int}\chi}$, which is smaller by a factor of 4. We used the susceptibility $\chi$ to determine the transition point.

We furthermore compute the Polyakov loop correlator $\langle L(\vec{s})L^{\dagger}(\vec{s}')\rangle$, from which we obtain the static potential. To reduce the error on the static potential, we employ a hypercubic blocking of the gauge field as described in [26]. We choose every 5th to 20th trajectory, depending on the value of $\kappa$, to compute the blocked Polyakov loop correlator.

We fix the MAG [6] by maximizing the gauge fixing functional $F(U)$,

$$F(U) = \frac{1}{12V}\sum_{s,\mu}(|U_{11}(s,\mu)|^2 + |U_{22}(s,\mu)|^2 + |U_{33}(s,\mu)|^2) \tag{4}$$

with respect to local gauge transformations $g$ of the lattice gauge field,

$$U(s,\mu) \rightarrow U^g(s,\mu) = g(s)^{\dagger}U(s,\mu)g(s+\hat{\mu}). \tag{5}$$

To do so, we use the simulated annealing (SA) algorithm. The advantage of this algorithm over the usual iterative procedure has been demonstrated in [16] for the MAG and in [27] for the maximal center gauge in the SU(2) gauge theory. In practice one does not find the global maximum of the gauge fixing functional in a finite-time computation. For this reason it has been proposed [16] to apply the SA algorithm to a number of randomly generated gauge copies and pick that one with the largest value of $F$. By increasing the number of gauge copies, one eventually reaches the situation, where the statistical noise is larger than the deviation from the global maximum. We use one gauge copy. We have checked that by increasing the number of gauge copies our results for the gauge dependent quantities are left unchanged within the error bars.

To obtain Abelian observables, one needs to project the SU(3) link matrices onto the maximal Abelian subgroup U(1) $\times$ U(1) first. The original construction [28] is equivalent to finding the Abelian gauge field $u(s,\mu) \in \mathrm{U}(1)\times\mathrm{U}(1)$ which maximizes $|\mathrm{Tr}(U(s,\mu)u^{\dagger}(s,\mu))|^2$. The Abelian counterpart of an observable is then obtained by substituting

$$u(s,\mu) = \mathrm{diag}(e^{i\theta_1(s,\mu)}, e^{i\theta_2(s,\mu)}, e^{i\theta_3(s,\mu)}), \tag{6}$$

for $U(s,\mu)$; $\sum_{i=1}^{3}\theta_i(s,\mu) = 0$, so that $\det(u(s,\mu)) = 1$. From Eq. (6) we define plaquette angles

$$\theta_i(s,\mu\nu) = \partial_{\mu}\theta_i(s,\nu) - \partial_{\nu}\theta_i(s,\mu), \tag{7}$$

where $\partial_{\mu}$ is the lattice forward derivative. The plaquette angles can be decomposed into regular and singular components,

$$\theta_i(s,\mu\nu) = \overline{\theta}_i(s,\mu\nu) + 2\pi m_i(s,\mu\nu), \tag{8}$$

where $\overline{\theta}_i(s,\mu\nu) \in (-\pi;\pi]$, and $m_i(s,\mu\nu) \in \mathbb{N}$ counts the number of Dirac strings piercing the given plaquette. Note that $\sum_i\overline{\theta}_i(s,\mu\nu) = 2\pi l$, $l = 0, \pm 1$. If $l = +1$ ($-1$) we substitute the largest (smallest) $\overline{\theta}_i(s,\mu\nu)$ (of the three components) by $\overline{\theta}_i(s,\mu\nu) - 2\pi$ ($+2\pi$), and similarly for $m_i(s,\mu\nu)$, so that $\sum_i\overline{\theta}_i(s,\mu\nu) = \sum_i m_i(s,\mu\nu) = 0$.

The monopole currents, being located on the links of the dual lattice, are defined by [29]

$$k_i(^*s,\mu) = \frac{1}{4\pi}\epsilon_{\mu\nu\rho\sigma}\partial_{\nu}\overline{\theta}_i(s+\hat{\mu},\rho\sigma) = -\frac{1}{2}\epsilon_{\mu\nu\rho\sigma}\partial_{\nu}m_i(s+\hat{\mu},\rho\sigma). \tag{9}$$

They satisfy the constraint

$$\sum_i k_i(^*s,\mu) = 0, \tag{10}$$

for any $^*s$, $\mu$. The Abelian gauge fields $\theta_i(s,\mu)$ can in turn be decomposed into monopole (singular) and photon (regular) parts:

$$\theta_i(s,\mu) = \theta_i^{\mathrm{mon}}(s,\mu) + \theta_i^{\mathrm{ph}}(s,\mu). \tag{11}$$

The monopole part is defined by [30]:

$$\theta_i^{\mathrm{mon}}(s,\mu) = -2\pi\sum_{s'}D(s-s')\partial'_{\nu}m_i(s',\nu\mu), \tag{12}$$

where $\partial'_{\nu}$ is the backward lattice derivative, and $D(s)$ denotes the lattice Coulomb propagator.

The Abelian Polyakov loop is defined by

$$L_{\mathrm{Abel}}(\vec{s}) = \frac{1}{3}\sum_{i=1}^{3}L_i^{\mathrm{Abel}}(\vec{s}), \qquad L_i^{\mathrm{Abel}}(\vec{s}) = \exp\left\{i\sum_{s_4=1}^{N_t}\theta_i(s,4)\right\}. \tag{13}$$

Similarly, we define the monopole and photon Polyakov loops [31]:

$$L_{\mathrm{mon}}(\vec{s}) = \frac{1}{3}\sum_{i=1}^{3}L_i^{\mathrm{mon}}(\vec{s}), \qquad L_i^{\mathrm{mon}}(\vec{s}) = \exp\left\{i\sum_{s_4=1}^{N_t}\theta_i^{\mathrm{mon}}(s,4)\right\}, \tag{14}$$

$$L_{\mathrm{ph}}(\vec{s}) = \frac{1}{3}\sum_{i=1}^{3}L_i^{\mathrm{ph}}(\vec{s}), \qquad L_i^{\mathrm{ph}}(\vec{s}) = \exp\left\{i\sum_{s_4=1}\theta_i^{\mathrm{ph}}(s,4)\right\}. \tag{15}$$

## III. TRANSITION TEMPERATURE

The order parameter of the finite temperature phase transition in quenched QCD is the Polyakov loop, and the corresponding symmetry is global $Z(3)$. In the presence of dynamical ''chiral'' fermions the chiral condensate $\langle\bar{\psi}\psi\rangle$ is an order parameter (of the chiral symmetry breaking transition). It is expected that there is no phase transition at

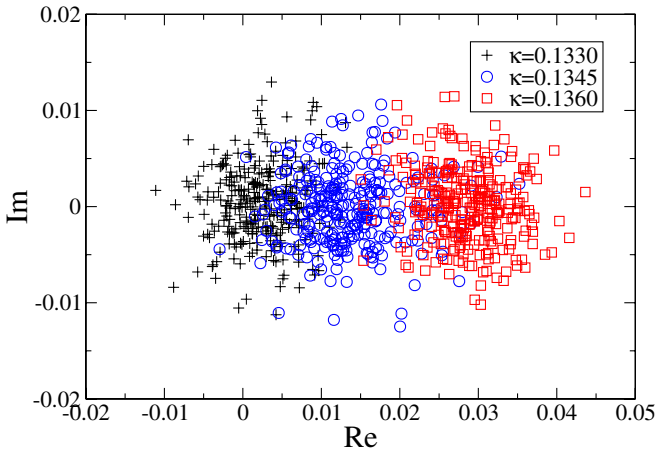


FIG. 2 (color online). Scatter plots of the Polyakov loop in the complex plane for various temperatures.

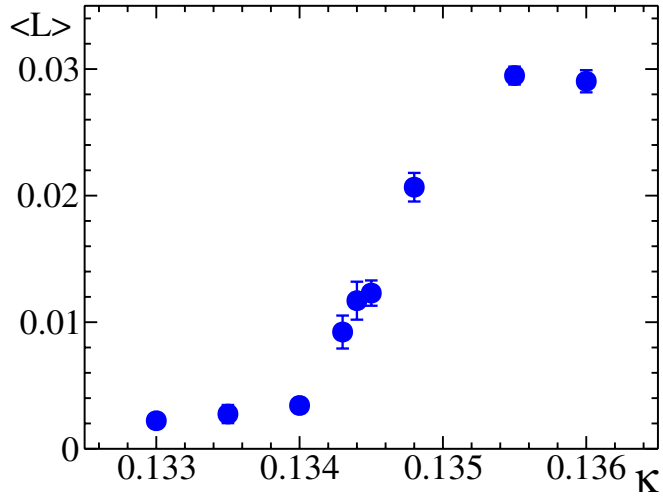


FIG. 3 (color online). The expectation value of the non-Abelian Polyakov loop as a function of $\kappa$.

intermediate quark masses, only a crossover. Numerical results show that both order parameters can be used to locate the transition point at intermediate quark masses [1]. We use the Polyakov loop, because the calculation of the chiral condensate for Wilson fermions requires renormalization and is rather involved.

It is instructive to plot the Polyakov loop in the complex plane as a function of temperature, which has been done in Fig. 2. We find that the distribution is rather asymmetric, even at the lowest temperature, favoring a positive value of Re$L$. This is indeed what one expects [32]. The introduction of dynamical quarks adds a term proportional to Re$L$ to the effective action, which results in a nonzero value of $\langle L \rangle$. The numbers are given in Table II.

In Table II we also give values for the Abelian and monopole Polyakov loops separately.

As we can see from Fig. 1, increasing $\kappa$ at a fixed value of $\beta$ increases the temperature $T \propto r_0/a$. In Figs. 3–5 we plot the expectation values of the various Polyakov loops of Table II as a function of $\kappa$. While $\langle L \rangle$, $\langle L_{\mathrm{Abel}} \rangle$ and $\langle L_{\mathrm{mon}} \rangle$ increase with increasing $\kappa$, $\langle L_{\mathrm{ph}} \rangle$ stays approximately constant over the full range of $\kappa$. Furthermore, similar to the quenched theory, $L_{\mathrm{mon}}$ and $L_{\mathrm{ph}}$ are virtually independent, which follows from $\langle L_{\mathrm{Abel}} \rangle \approx \langle L_{\mathrm{mon}} \rangle \langle L_{\mathrm{ph}} \rangle$.

The task is now to determine the transition temperature $T_c$. We call the $\kappa$ value, at which the transition takes place, $\kappa_t$. We identify $\kappa_t$ as the point, where the Polyakov loop susceptibility (3) assumes its maximum. The precise value is obtained by applying a Gaussian fit to the neighboring points. The Abelian, monopole and photon Polyakov loop susceptibilities $\chi_{\mathrm{Abel}}$, $\chi_{\mathrm{mon}}$ and $\chi_{\mathrm{ph}}$, respectively, are defined similarly to (3). The susceptibilities are given in Table III, and they are plotted in Figs. 6 and 7 together with the Gaussian fit. From the non-Abelian susceptibility $\chi$ we find $\kappa_t = 0.13444(6)$. To obtain the value of the critical temperature in physical units we first compute the dimensionless number

TABLE II. The expectation values of the non-Abelian, Abelian, monopole and photon Polyakov loops at $\beta = 5.2$.

| $\kappa$ | $\langle L \rangle$ | $\langle L \rangle_{\mathrm{Abel}}$ | $\langle L \rangle_{\mathrm{mon}}$ | $\langle L \rangle_{\mathrm{ph}}$ | $T/T_c$ |
|---|---|---|---|---|---|
| 0.1330 | 0.0022(3) | 0.014(2) | 0.040(7) | 0.2946(10) | 0.798 |
| 0.1335 | 0.0027(7) | 0.018(5) | 0.054(16) | 0.3007(9) | 0.863 |
| 0.1340 | 0.0034(5) | 0.025(4) | 0.079(14) | 0.3052(7) | 0.934 |
| 0.1343 | 0.0092(13) | 0.074(11) | 0.235(35) | 0.3113(6) | 0.979 |
| 0.1344 | 0.0117(15) | 0.095(13) | 0.310(42) | 0.3102(5) | 0.994 |
| 0.1345 | 0.0123(10) | 0.100(9) | 0.328(28) | 0.3114(4) | 1.010 |
| 0.1348 | 0.0207(11) | 0.169(10) | 0.556(32) | 0.3197(9) | 1.058 |
| 0.1355 | 0.0300(7) | 0.235(5) | 0.740(11) | 0.3279(9) | 1.178 |
| 0.1360 | 0.0290(9) | 0.236(6) | 0.747(11) | 0.3291(14) | 1.271 |

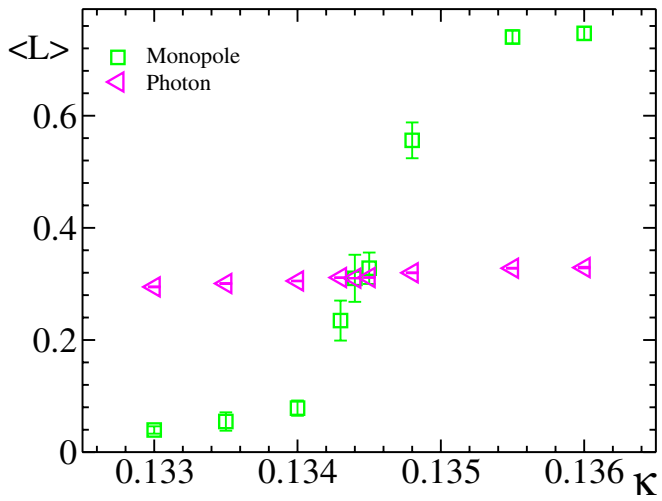


FIG. 4 (color online). The expectation value of monopole and photon Polyakov loops as functions of $\kappa$.

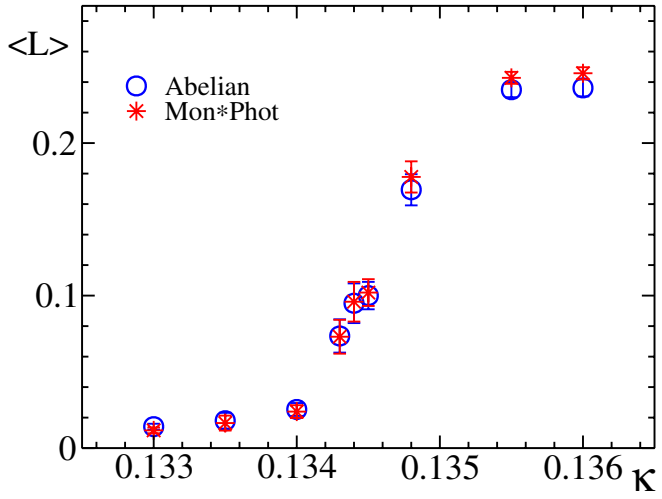


FIG. 5 (color online). The expectation value of the Abelian Polyakov loop as a function of $\kappa$. The product of monopole and photon Polyakov loops is also shown.

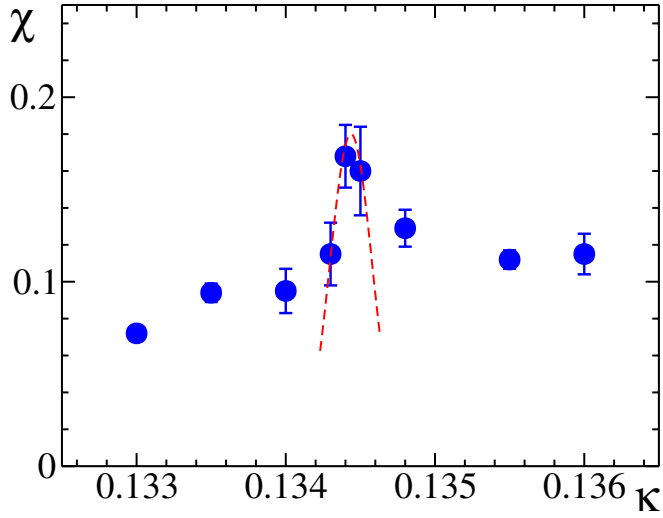


FIG. 6 (color online). The non-Abelian Polyakov loop susceptibility as a function of $\kappa$ together with the fit.

$$Tr_0 \equiv \frac{r_0}{8a}. \tag{16}$$

We get $T_c r_0 = 0.536(8)$, where the value of $r_0/a$ at $\kappa_t$ have been obtained by interpolation of the $T = 0$ results [20]. The error of $T_c r_0$ includes both the error of $\kappa_t$ and that of $r_0/a$. Taking $r_0^{-1} = 395$ MeV to fix the scale, we obtain in physical units

$$T_c = 212(4)\ \text{MeV}, \qquad \frac{m_\pi}{m_\rho} = 0.77. \tag{17}$$

Here the $m_\pi/m_\rho$ ratio was obtained by interpolation of the $T = 0$ data [20]. Similarly, we can compute the temperature $T$ at our various $\kappa$ values. The result is given in the last column of Table II in the form of

$$\frac{T}{T_c} \equiv \frac{Tr_0|_\kappa}{Tr_0|_{\kappa_t}}. \tag{18}$$

The statistical error of this ratio is about 2% for all data sets. It should be noted that the numbers given in Eq. (17) depend on the physical quantity to fix the scale. This uncertainty will disappear only in the chiral and perhaps the continuum limit. Experience shows, however, that $r_0 = 0.5$ fm is a reasonable choice even at our quark masses.

The susceptibilities $\chi_{\text{Abel}}$ and $\chi_{\text{mon}}$ have maxima at the same $\kappa$ value as the non-Abelian susceptibility. The Gaussian fits for the Abelian and monopole susceptibilities give $\kappa_t$ values which agree within error bars with $\kappa_t$ determined from the non-Abelian susceptibility. We find that $\chi_{\text{Abel}} \approx \langle L_{\text{ph}} \rangle^2 \chi_{\text{mon}}$. This follows from our earlier observation, namely, that $L_{\text{mon}}$ and $L_{\text{ph}}$ are independent, and the smallness of $\chi_{\text{ph}}$. The non-Abelian susceptibility is 10 to 50 times smaller than its Abelian counterpart. The photon susceptibility does not show any change at the

TABLE III. The expectation values of the susceptibility of the non-Abelian, Abelian, monopole and photon Polyakov loop.

| $\kappa$ | $\chi$ | $\chi_{\text{Abel}}$ | $\chi_{\text{mon}}$ | $\chi_{\text{ph}}$ |
|---|---|---|---|---|
| 0.1330 | 0.072(3) | 0.88(10) | 7.7(8) | 0.590(16) |
| 0.1335 | 0.094(5) | 1.8(3) | 17.4(2.4) | 0.624(10) |
| 0.1340 | 0.095(12) | 2.4(5) | 25.5(4.9) | 0.638(12) |
| 0.1343 | 0.115(17) | 4.2(1.1) | 46.1(12) | 0.653(10) |
| 0.1344 | 0.168(17) | 8.4(1.3) | 97.2(17) | 0.777(10) |
| 0.1345 | 0.160(24) | 7.5(1.3) | 82.6(12) | 0.760(13) |
| 0.1348 | 0.129(10) | 5.7(8) | 57.5(9.4) | 0.705(25) |
| 0.1355 | 0.112(5) | 2.7(4) | 17.7(2.2) | 0.686(27) |
| 0.1360 | 0.115(11) | 2.3(5) | 14.7(2.8) | 0.734(29) |

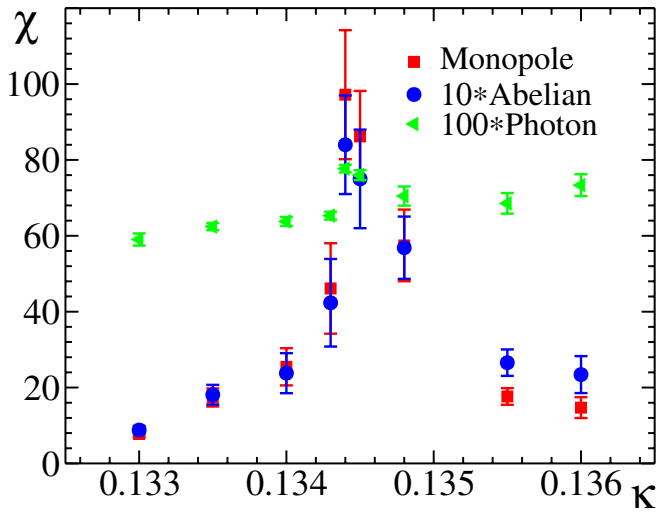


FIG. 7 (color online). The same as in Fig. 6 but for the Abelian, the monopole and the photon Polyakov loop susceptibilities. The Abelian (photon) Polyakov loop susceptibility has been enhanced by a factor of 10 (100).

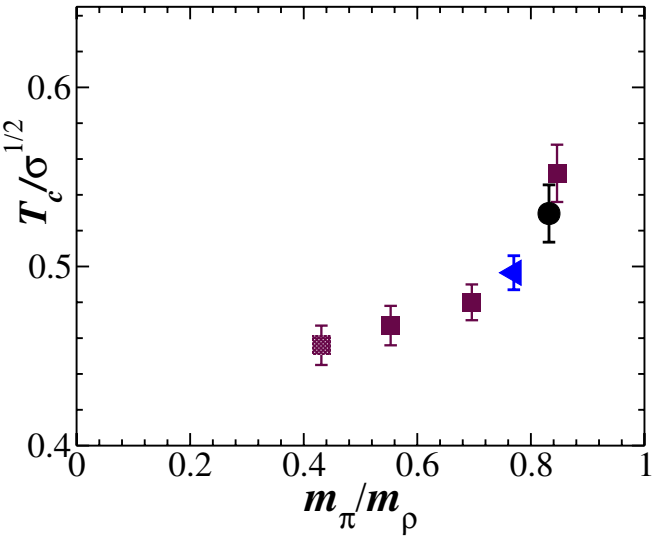


FIG. 8 (color online). The transition temperature as a function of $m_\pi/m_\rho$ from this work (triangle), from [1] (squares), and from [22] (circle).

critical temperature, as expected. We conclude, that the monopole degrees of freedom are most sensitive to the transition, as was the case in the quenched theory.

In Fig. 8 we compare our result for $T_c/\sqrt{\sigma}$ with those of Refs. [1,22], where we have assumed $\sqrt{\sigma} = 425$ MeV. Our result is in quantitative agreement with the results of the Bielefeld group. This is reassuring, as [1,22] work at larger lattice spacing. Comparing with another work [33], where an improved gauge and a clover improved fermion actions with tadpole improved coefficients were used, we find that our value is essentially higher.

Because $N_s/N_t = 2$ in our simulations, the question of finite volume effects is essential. To check for finite volume effects we have performed simulations at $\beta = 5.2$, $\kappa = 0.1343$ on $24^3 \times 8$ lattices. The value of $\kappa$ was chosen close to the transition point, where finite volume corrections are expected to be largest. We found $\langle L \rangle = 0.0098(10)$ and $\chi = 0.099(13)$, as compared to $\langle L \rangle = 0.0092(13)$ and $\chi = 0.115(17)$, respectively, on the $N_s = 16$ lattice. In both cases the numbers agree within the error bars, so that we do not reckon with large effects. This agrees with observation [1] that in $N_f = 2 + 1$ QCD finite size effects for $\chi$ are small at $m_\pi/m_\rho < 0.9$.

## IV. HEAVY QUARK POTENTIAL

### A. Ansatz

One of the characteristic features of full QCD is breaking of the string spanned between static quark and antiquark pairs. String breaking will manifest itself in a type of screening behavior of the heavy quark potential. At zero temperature no clear evidence for string breaking has been found (in QCD) yet. The reason is, so it is believed, that the Wilson loop has very small overlap with the broken string state. The expectation value of the Wilson loop for large distances $r$ can be written as

$$\langle W(r,t) \rangle = C_V(r) e^{-(V_0 + V_{\text{string}}(r))t} + C_E(r) e^{-2E_{sl} \cdot t} + ..., \tag{19}$$

where $V_{\text{string}}(r)$ is the usual confining potential, $V_{\text{string}}(r) = -\alpha/r + \sigma r$, $E_{\text{sl}}$ is the static-light meson energy, and $V_0$ is the self-energy. The latter is divergent in the continuum limit $a \to 0$. The overlap with the string state, $C_V(r)$, is of the order of 1, while the overlap with the broken string, $C_E(r)$, appears to be small. An estimate [34] is: $C_E(r) \sim e^{-2m_{sl} \cdot r}$, where $m_{sl} = E_{sl} - V_0/2$ is the so called binding energy of the static-light meson or, in other words, the constituent quark mass [35]. (See also the discussion in Ref. [36].) A similar estimate was given in Ref. [37], based on the hypothesis of Abelian dominance.

The conventional definition of the string breaking distance is the distance $r_{sb}$, at which the energy of two static-light mesons is equal to the energy of the string, i.e.

$$2m_{sl} = \sigma \cdot r_{sb} - \frac{\pi}{12 r_{sb}}. \tag{20}$$

The Wuppertal group found $r_{sb} = 2.3 r_0$ at $m_\pi/m_\rho = 0.7$ [3], while CP-PACS found $r_{sb} = 2.2 r_0$ at $m_\pi/m_\rho = 0.6$ [34]. In full QCD it was found $\sqrt{\sigma} r_0 = 1.14$ [3] and $\sqrt{\sigma} r_0 = 1.16$ [21], respectively, from which we derive $2m_{sl} \approx 2.9/r_0 \approx 1.1$ GeV, assuming $r_0 = 0.5$ fm. This agrees with the estimate of [38]. Using these values for $\sqrt{\sigma} r_0$ and $m_{sl}$ and assuming the mentioned above form of $C_E(r)$ we can estimate the values of $r$ and $t$ at which the two terms in Eq. (19) become equal indicating that the string breaking effects become visible:

$$r = t = \frac{4 m_{sl}}{\sigma}. \tag{21}$$

We also estimate the numerical value of the Wilson loop of the corresponding size:

$$\langle W(r,t) \rangle \lesssim 10^{-11} \cdot e^{-V_0 t}. \tag{22}$$

It is a challenging task to record a Wilson loop of this order of magnitude. Recently, a first successful attempt to do so was reported in [39] where the authors studied the adjoint static potential in three-dimensional SU(2) gauge theory.

At finite temperature $T < T_c$ string breaking has been studied in [40]. The heavy quark potential $V(r,T)$ is obtained from the Polyakov loop correlator:

$$\frac{1}{T} V(r,T) = -\ln \langle L(\vec{s}) L^\dagger(\vec{s}\,') \rangle, \tag{23}$$

up to an entropy contribution, where $r = |\vec{s} - \vec{s}\,'|$. At large separations

$$\langle L(\vec{s}) L^\dagger(\vec{s}\,') \rangle \xrightarrow[|\vec{s} - \vec{s}\,'| \to \infty]{} |\langle L \rangle|^2, \tag{24}$$

where $|\langle L \rangle|^2 \neq 0$, as global $Z_3$ is broken by fermions. It

should be noted that the potential in (23) is a proper color singlet potential [41].

The spectral representation of the Polyakov loop correlator is given by [42]

$$\langle L(\vec{s})L^\dagger(\vec{s}')\rangle = \sum_{n=0}^{\infty} w_n e^{-E_n(r)/T}, \tag{25}$$

where $w_n$ are integers. At zero temperature we have $V(r,0) = E_0(r)$, up to a constant, where $E_0$ is the ground state energy. At finite temperature $V(r,T)$ gets contributions from all (excited) states. As was discussed already, at $T = 0$ the potential can be described by the string model potential up to the string breaking distance $r_{sb}$. Beyond this distance the state of two static-light mesons becomes the ground state of the system. Thus, there are two competing states in the spectrum, and it depends on the distance $r$, which one will be the ground state. We may expect that the situation at small temperature is similar to the case of $T = 0$.

We shall now assume that at temperatures $T < T_c$ the Polyakov loop correlator can be described in terms of these two states. We then have

$$\langle L(\vec{s})L^\dagger(\vec{s}')\rangle = e^{-(V_0(T)+V_{\rm string}(r,T))/T} + e^{-2E(T)/T}, \tag{26}$$

where the finite temperature string potential $V_{\rm string}(r,T)$ is given by [43]:

$$\begin{aligned} V_{\rm string}(r,T) = &-\frac{1}{r}\left(\alpha - \frac{1}{6}\arctan(2rT)\right) \\ &+ \left(\sigma(T) + \frac{2T^2}{3}\arctan\frac{1}{2rT}\right)r \\ &+ \frac{T}{2}\ln(1+4r^2T^2). \end{aligned} \tag{27}$$

We consider the temperature dependent string tension $\sigma(T)$, which according to [43] is equal to $\sigma(0) - \frac{\pi}{3}T^2$, as a free parameter. While in [43] $\alpha$ was fixed at $\pi/12$, a fit of the short distance part of the potential at $T = 0$ gave [44] $\alpha = 0.32 \sim 0.34$. In the following we shall consider both cases, $\alpha = \pi/12$ and $\alpha = 0.33$. The energy $E(T)$ can be written as

$$E(T) = \frac{1}{2}V_0(T) + m(T), \tag{28}$$

where $m(T)$ is the constituent quark mass [35].

A long time ago the following ansatz for the Polyakov loop correlator has been proposed [4]:

$$\langle L(\vec{s})L^\dagger(\vec{s}')\rangle = e^{-(V_0(T)+V_{\rm KMS}(r,T))/T}, \tag{29}$$

where

$$V_{KMS}(r,T) = \frac{\tilde{\sigma}}{\mu}(1-e^{-\mu r}) - \frac{\tilde{\alpha}}{r}e^{-\mu r}. \tag{30}$$

We do not consider this potential a valid ansatz, because string breaking is a level crossing phenomenon.

Besides the non-Abelian potential, we will study the Abelian one. In particular we shall be interested in its monopole and photon parts. From studies at zero temperature [12,16] it is known that the monopole part of the potential decreases linearly down to very small distances, showing no Coulomb term, which sometimes makes it easier to extract a string tension. It appears that the monopole part of the potential has not only no Coulomb term, but also shows no broadening of the flux tube as the length of the flux tube is increased. (Both phenomena are connected of course.) As we show below, our monopole potential is also linear at distances up to the distance of order of 0.5 fm where flattening starts. Thus we may write

$$\langle L_{\rm mon}(\vec{s})L^\dagger_{\rm mon}(\vec{s}')\rangle = e^{-(V_0^{\rm mon}(T)+V_{\rm string}^{\rm mon}(r,T))/T} + e^{-2E_{\rm mon}(T)/T}, \tag{31}$$

where

$$\begin{aligned} V_{\rm string}^{\rm mon}(r,T) &= \sigma_{\rm mon}\cdot r, \\ E_{\rm mon}(T) &= \frac{1}{2}V_0^{\rm mon}(T) + m_{\rm mon}(T). \end{aligned} \tag{32}$$

### B. Hypercubic blocking

As was mentioned already, we apply hypercubic blocking (HCB) [26] to reduce the statistical errors. That means every SU(3) link matrix $U(s,\mu)$ is replaced by a new link matrix $U_{\rm HCB}(s,\mu)$, which is the weighted sum of products of link matrices along paths from $s$ to $s+\hat{\mu}$ within adjacent cubes projected onto the nearest SU(3) group element. We used the same parameters as in [26].

In Fig. 9 we compare the static potential from blocked and unblocked configurations. We see that the statistical errors are substantially reduced. Furthermore, rotational invariance is improved, in agreement with earlier observa-

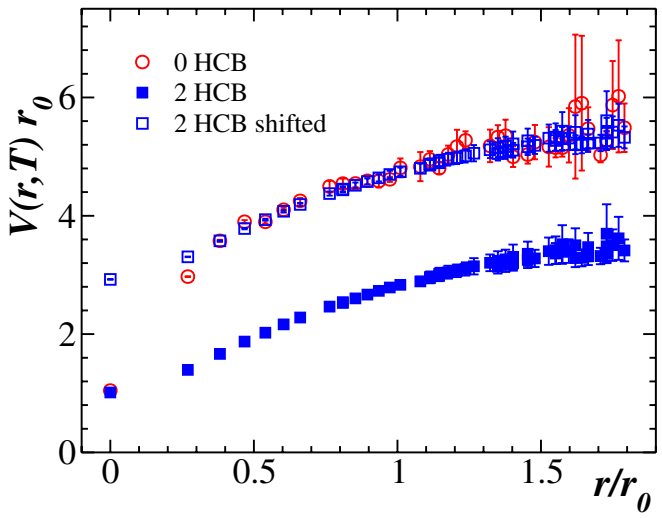


FIG. 9 (color online). Effect of hypercubic blocking on the potential at $\beta = 5.2$, $\kappa = 0.1335$.

tions [26]. The blocking procedure decreases the self-energy of the static sources, which causes a constant shift in the potential. In Fig. 9 we shift the potential by $1.33/r_0$, so that it agrees with the unblocked potential at $r = \sqrt{2}a$. We find good agreement at all distances, except perhaps at $r = a$. The shift agrees with the change in the asymptotic value of the potential, $-2T\log\langle L\rangle$, which was found to be $1.24(25)/r_0$. The discrepancy at $r = a$ can be accounted for by perturbative corrections [45]. All our fits are made for $r/r_0 \geq 1$ thus this point is always discarded.

### C. Non-Abelian potential

We first fit the static potential by the two-state ansatz (26). This is done for two different choices of $\alpha$, $\alpha = \pi/12$ and $\alpha = 0.33$. Examples of the fit for $TT_c = 0.863$ and 0.979 and the second choice $\alpha = 0.33$ are shown in Fig. 10. The curves for $\alpha = \pi/12$ and $\alpha = 0.33$ are practically indistinguishable from each other, visually and in terms of $\chi^2$/dof. We also show the asymptotic value of the potential, $-2T\ln\langle L\rangle$. The potential converges to this value at large distances. The two-state ansatz describes the data very well. The fit parameters are given in Table IV, where $\sigma(0) = (1.14/r_0)^2$ [3] was used.

The string tension $\sigma(T)$ and the constituent quark mass $m(T)$ are plotted in Figs. 11 and 12, respectively.

In Fig. 11 the quenched value of $\sigma(T)/\sigma(0)$ [Eq. (15) from [46] ] is shown for comparison. Both the string tension and the constituent quark mass decrease with increasing temperature, as we expect. The results differ by approximately one $\sigma$ between $\alpha = 0.33$ and $\alpha = \pi/12$. For lower temperature, at $T/T_c = 0.798$, we find rather good agreement for the string tension between the results of the quenched theory and our results obtained with the choice $\alpha = 0.33$. For higher temperatures agreement is much worse. While our results for $\sigma(T)/\sigma(0)$ agree with predictions of the effective string model [47], $1 - (\pi T^2/3\sigma(0))$, as is seen from Fig. 11, the quenched results lie much lower. Note, however, that for equal values of the ratio $T/T_c$ our results are obtained at temperatures essentially lower than the temperatures in quenched QCD. Indeed, the critical temperature $T_c = 212$ MeV is about 0.8 of the quenched critical temperature.

The difference in behavior of the ratio $\sigma(T)/\sigma(0)$ as function of $T/T_c$ between quenched and full QCD might

TABLE IV. Fit parameters of the two-state ansatz (26), where we have assumed $\sigma(0) = (1.14/r_0)^2$.

| $T/T_c$ | $V_0 r_0$ | $\sigma(T)/\sigma(0)$ | $m(T)r_0$ |
|---|---|---|---|
| | $\alpha = 0.33$ | | |
| 0.798 | 1.62(1) | 0.86(2) | 1.04(8) |
| 0.863 | 1.79(3) | 0.83(4) | 0.86(10) |
| 0.934 | 1.97(3) | 0.82(4) | 0.77(7) |
| 0.979 | 2.10(5) | 0.76(7) | 0.51(8) |
| | $\alpha = \pi/12$ | | |
| 0.798 | 1.44(1) | 0.95(2) | 1.10(8) |
| 0.863 | 1.59(3) | 0.94(4) | 0.95(10) |
| 0.934 | 1.77(3) | 0.94(4) | 0.87(7) |
| 0.979 | 1.90(5) | 0.88(8) | 0.61(8) |
| | Monopole part | | |
| 0.798 | 0.47(1) | 0.90(1) | 1.24(4) |
| 0.863 | 0.53(1) | 0.85(1) | 1.07(2) |
| 0.934 | 0.61(1) | 0.84(1) | 1.03(3) |
| 0.979 | 1.06(1) | 0.46(1) | 0.21(1) |

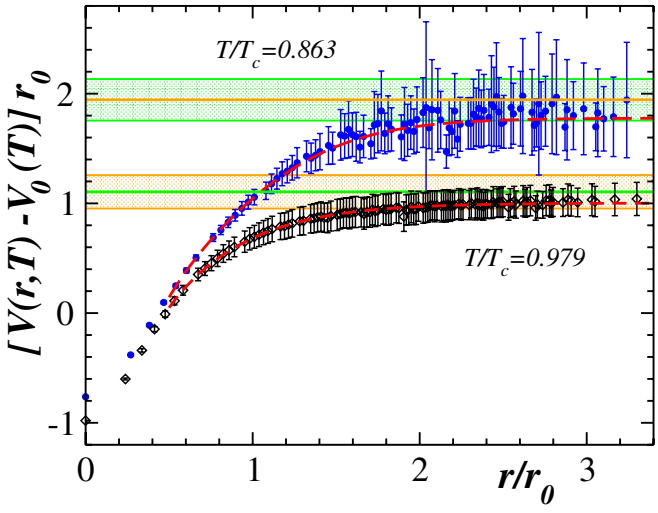


FIG. 10 (color online). The heavy quark potential at $\beta = 5.2$ for $T/T_c = 0.863$ and 0.979, together with the fit using $\alpha = 0.33$. The horizontal lines show the asymptotic value of the potential, where the shaded area indicates the error.

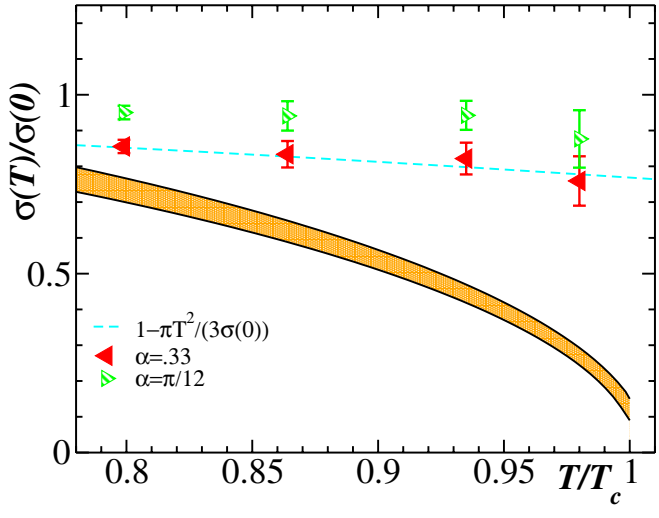


FIG. 11 (color online). The string tension from a fit of the two-state ansatz (26) as a function of temperature. The quenched value of the string tension [46] is shown for comparison with the shaded area indicating the error bar. The upper (dashed) curve shows the prediction of the effective string model [47].

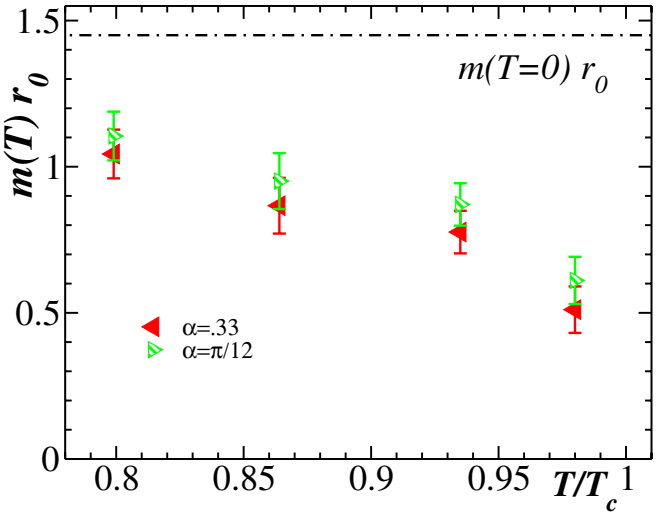


FIG. 12 (color online). The constituent quark mass from a fit of the two-state ansatz (26) as a function of temperature. The dash-dotted line indicates the zero-temperature value of the mass $m_{sl}$.

be a consequence of the difference in the nature of the transition: while in quenched QCD the transition is first order, in full QCD at intermediate quark masses the transition is a crossover. Note that at a crossover all quantities change smoothly and, consequently, the string tension should not vanish at $T = T_c$ in our case. We assume from Fig. 11 that the string tension continues to decrease smoothly as temperature goes above $T_c$. However, the very notion of the string for $T \approx T_c$ seems to be out of the physical relevance due to the very low value of the string breaking distance $r_{sb}$, see Fig. 15 below.

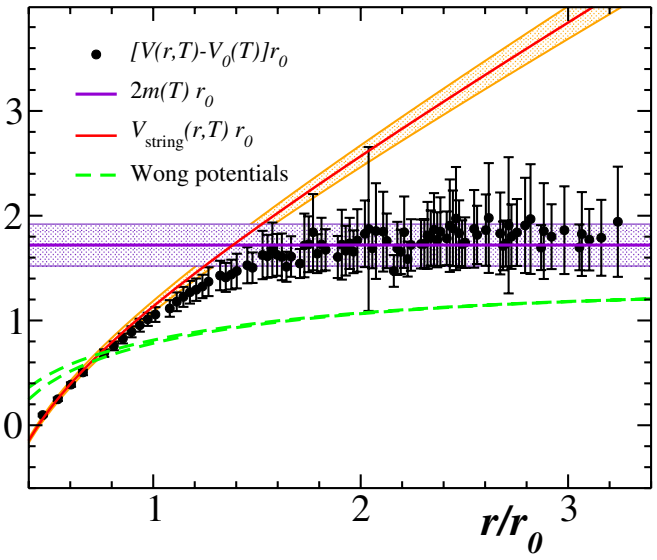


FIG. 13 (color online). The string potential and the constituent mass as a function of distance at $\beta = 5.2$ for $\kappa = 0.1335$ ($T/T_c = 0.863$). The shaded regions indicate the errors.

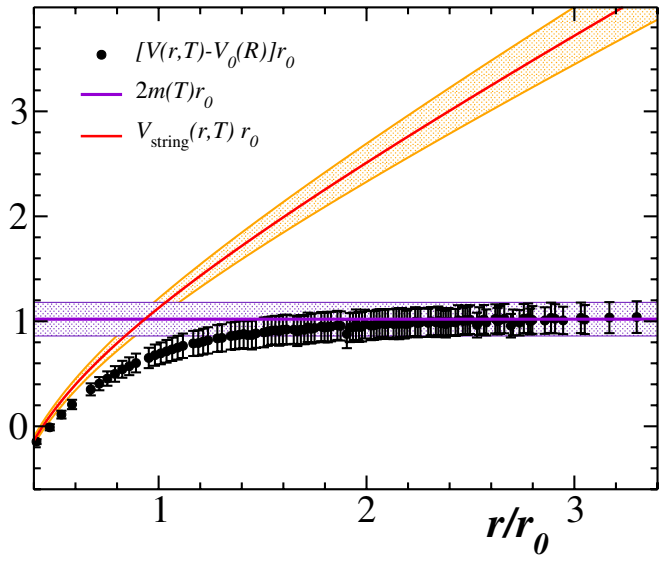


FIG. 14 (color online). The same as in Fig. 13 but for $\kappa = 0.1343$ ($T/T_c = 0.979$).

Our values for the constituent quark mass $m(T)$ are larger by about 100 MeV than those reported in [38]. However, one should note a difference between our definition of the self-energy and the definition used in Ref. [38].

We are now able to compute the string breaking distance $r_{sb}$ from

$$V_{\text{string}}(r_{sb}, T) = 2m(T). \tag{33}$$

In Figs. 13 and 14 we show the two energy levels together with the data. The string breaks where the two levels cross. The dependence of $r_{sb}$ on the temperature is shown in Fig. 15. We see that $r_{sb}$ decreases as the temperature is

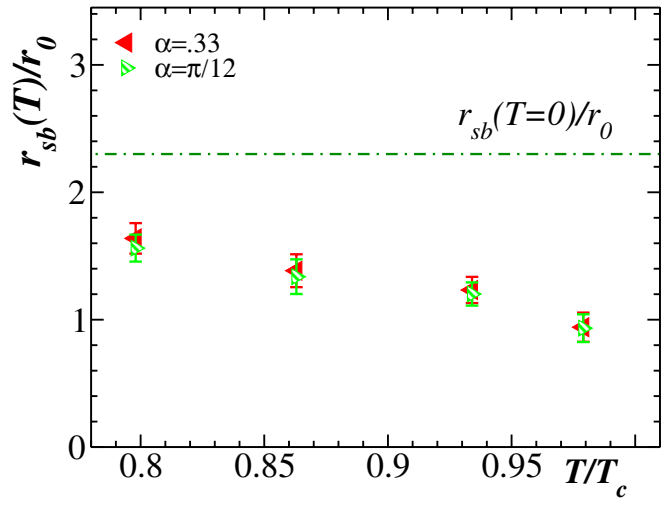


FIG. 15 (color online). The string breaking distance $r_{sb}$ as a function of temperature. The dash-dotted line indicates the corresponding zero-temperature value [3].

increased. The difference of $r_{sb}$ between the two choices of $\alpha$ lies within the error bars.

Let us now consider the screening potential (30). Fitting this potential to our data gives a comparable value of $\chi^2/\mathrm{dof}$. However, the parameters of the fit turn out to be unphysical. For example, at $T/T_c = 0.798$, 0.863 and 0.934 we obtain $\tilde{\sigma}/\sigma(0) = 21(6)$, 13(2) and 5.5(6), respectively. Only close to the deconfinement transition we do find a reasonable value for the string tension: $\tilde{\sigma}/\sigma(0) = 0.4(3)$ at $T/T_c = 0.979$.

The screening potential (30) may be rewritten (up to a constant) in the following form [48]:

$$V^{\mathrm{Wong}}(r,T) = \left[-\frac{4}{3}\frac{\alpha_s}{r} - \frac{b(T)}{\mu_0}\right]e^{-\mu_0 r}. \qquad (34)$$

Taking (as in [48]) $b(T) = b_0(1-(T/T_c)^2)$, $b_0 = 0.35\ \mathrm{GeV}^2$, $\mu_0 = 0.28$ GeV, and $\alpha_s \sim 0.32$ ($\alpha_s \sim 0.24$) for the charmonium (bottonium) potential, and shifting the potential by a constant so that it agrees with the lattice potential at $r = r_0$, we find no agreement between this potential and the lattice data. Thus, the potential used in [48] to compute the quarkonium spectrum at finite temperature hardly agrees with the lattice static potential. The discrepancy is largest at smaller distances, where it matters most. It is unlikely that the situation will change with smaller quark masses.

### D. Monopole part of the potential

We carried out a similar analysis as before for the monopole part of the heavy quark potential, which is obtained from the correlator (31). The fit parameters are given in Table IV, and the potential is shown in Fig. 16. The errors are smaller than in the previous fits, as expected. The monopole part of the potential shows no Coulomb term, while at large distances it converges to its asymptotic value $-2T\ln\langle L_{\mathrm{mon}}\rangle$.

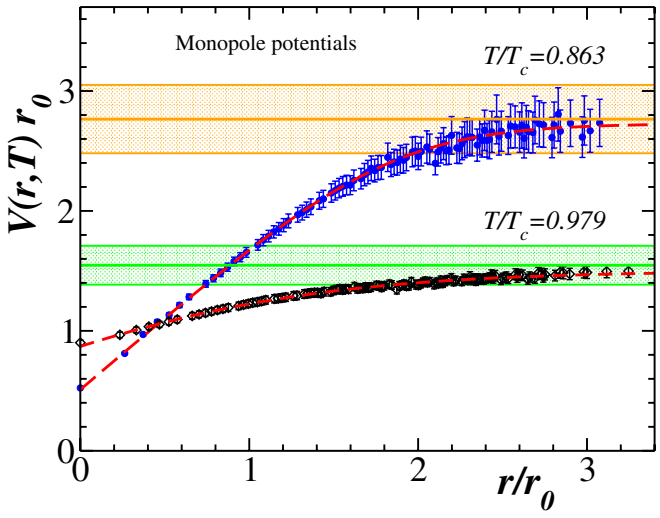


FIG. 16 (color online). The monopole part of the potential as a function of distance at $\beta = 5.2$ for $T/T_c = 0.863$ and 0.979, together with a fit of the form (32) (dashed curve). The horizontal lines show the asymptotic value of the potential, where the shaded area indicates the error.

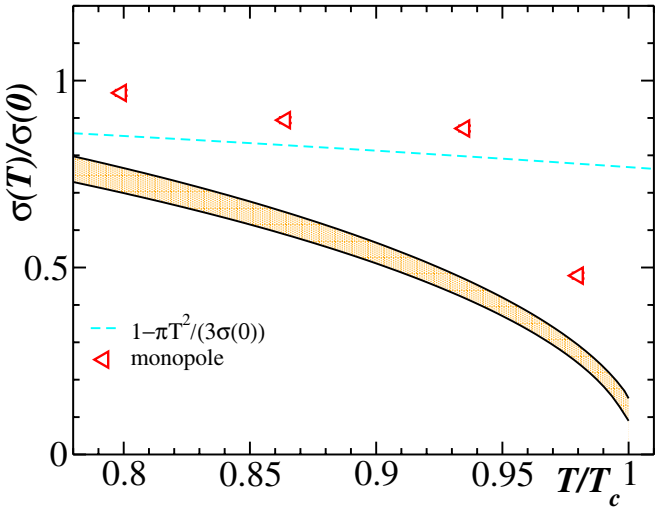


FIG. 17 (color online). The string tension of the monopole part of the potential as a function of temperature. The curves are the same as in Fig. 11.

The string tension $\sigma_{\mathrm{mon}}(T)$ and the constituent quark mass $m_{\mathrm{mon}}(T)$ are shown in Figs. 17 and 18, respectively. Because the Coulomb term is absent, we now can determine the string tension much more accurately. We find substantially larger values than in the quenched case. Furthermore, the string tension appears to decrease more slowly as the system is heated. The constituent quark mass $m_{\mathrm{mon}}(T)$ looks very much the same as in the non-Abelian case. The same holds for the string breaking distance, $r_{sb}^{\mathrm{mon}}$, which is shown in Fig. 19.

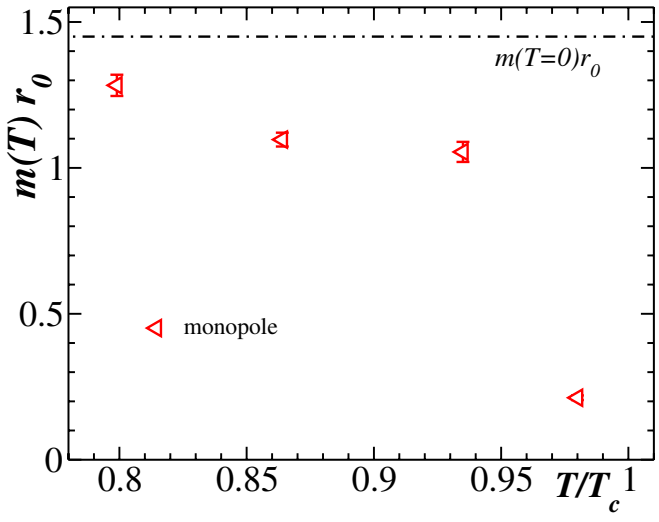


FIG. 18 (color online). The same as in Fig. 17 but for the constituent quark mass. The dash-dotted line indicates the zero-temperature value of the mass $m_{sl}$.

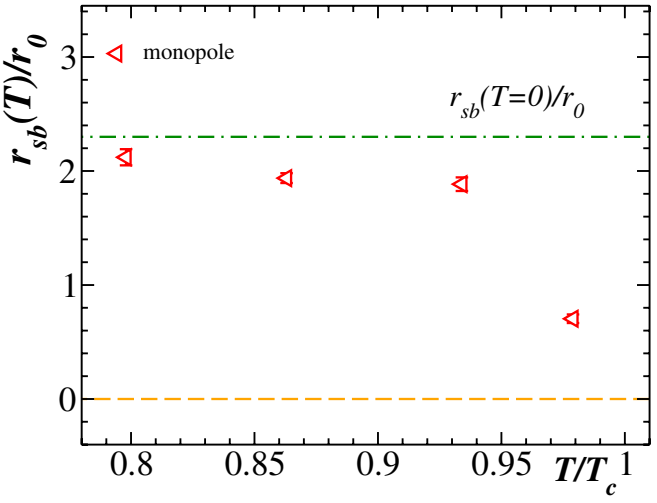


FIG. 19 (color online). The string breaking distance $r_{sb}^{\rm mon}$ obtained from the monopole potential as a function of temperature. The dash-dotted line indicates the corresponding zero-temperature value [3].

To shed further light on the string breaking mechanism, we have computed the action density, the color electric field and the monopole current in the vicinity of the (broken) string.

The definitions of observables are the same as in Ref. [12]. We are interested in local Abelian operators of the form:

$$\mathcal{O}(s) = \mathrm{diag}(\mathcal{O}_1(s), \mathcal{O}_2(s), \mathcal{O}_3(s)) \in \mathrm{U}(1) \times \mathrm{U}(1). \quad (35)$$

The correlator of the action density—which is $C$-parity even operator—with the product of the monopole Polyakov loops, $\mathcal{L}_{\rm mon}(\vec{s}')\mathcal{L}^\dagger_{\rm mon}(\vec{s}'')$, can be written analogously to Ref. [49]:

$$\langle \mathcal{O}(s)\rangle_{\mathcal{L}_{\rm mon}} \equiv \frac{1}{3}\frac{\langle \mathrm{Tr}\mathcal{O}(s)\mathrm{Tr}[\mathcal{L}_{\rm mon}(\vec{s}')\mathcal{L}^\dagger_{\rm mon}(\vec{s}'')]\rangle}{\langle \mathrm{Tr}[\mathcal{L}_{\rm mon}(\vec{s}')\mathcal{L}^\dagger_{\rm mon}(\vec{s}'')]\rangle} - \frac{1}{3}\langle \mathrm{Tr}\mathcal{O}\rangle, \quad (36)$$

where

$$\mathcal{L}_{\rm mon}(s) = \mathrm{diag}(L_1^{\rm mon}(s), L_2^{\rm mon}(s), L_3^{\rm mon}(s)), \quad (37)$$

[cf. Eq. (14)].

As for the $C$-parity odd operators $\mathcal{O}$, such as the color electric field and the monopole current, we have

$$\langle \mathcal{O}(s)\rangle_{\mathcal{L}_{\rm mon}} \equiv \frac{\langle \mathrm{Tr}(\mathcal{O}(s)[\mathcal{L}_{\rm mon}(\vec{s}')\mathcal{L}^\dagger_{\rm mon}(\vec{s}'')])\rangle}{\langle \mathrm{Tr}[\mathcal{L}_{\rm mon}(\vec{s}')\mathcal{L}^\dagger_{\rm mon}(\vec{s}'')]\rangle}, \quad (38)$$

in analogy to the case of SU(2) and U(1) theories, Refs. [50].

The monopole part of the action density $\rho_A^{\mathcal{L}_{\rm mon}}$, the monopole part of the color electric field $E_i^{\mathcal{L}_{\rm mon}}$ and the monopole current $k^{\mathcal{L}_{\rm mon}}$, induced by the Polyakov loops, are then given by

$$\rho_A^{\mathcal{L}_{\rm mon}}(s) = \frac{\beta}{3}\sum_{\mu>\nu}\langle \mathrm{diag}(\cos(\theta_1^{\rm mon}(s,\mu,\nu)), \cos(\theta_2^{\rm mon}(s,\mu,\nu)), \cos(\theta_3^{\rm mon}(s,\mu,\nu)))\rangle_{\mathcal{L}_{\rm mon}}, \quad (39)$$

where the plaquette angles, $\theta_i^{\rm mon}(s,\mu,\nu)$, are constructed from the monopole link angles (12),

$$E_j^{\mathcal{L}_{\rm mon}}(s) = i\langle \mathrm{diag}(\theta_1^{\rm mon}(s,4,j), \theta_2^{\rm mon}(s,4,j), \theta_3^{\rm mon}(s,4,j))\rangle_{\mathcal{L}_{\rm mon}}, \quad (40)$$

and

$$k^{\mathcal{L}}({}^*s,\mu) = 2\pi i\langle \mathrm{diag}(k_1({}^*s,\mu), k_2({}^*s,\mu), k_3({}^*s,\mu))\rangle_{\mathcal{L}_{\rm mon}}, \quad (41)$$

respectively.

In Fig. 20 we show the result for $T/T_c = 0.979$ and three different separations, $r = 0.5$, 0.8 and 1.3 fm. Our estimate of the string breaking distance at this temperature is $\approx 0.5$ fm. The figure suggests that the flux tube has disappeared at the latest at $r = 1.3$ fm.

## V. MONOPOLE DENSITY

Another characteristic quantity of the confining vacuum is the monopole density, which we define as

$$\rho = \frac{1}{12N_tN_s^3}\left\langle \sum_{i=1}^{3}\sum_{s,\mu}|k_i({}^*s,\mu)|\right\rangle, \quad (42)$$

where the monopole current, $k_i({}^*s,\mu)$, is given in (9).

In Fig. 21 we compare the monopole density of this work with that of the quenched theory. The quenched result has been obtained on the same sized lattice at $\beta = 5.8$, 5.9, 6.0, 6.1 and 6.2. The density in full QCD is substantially higher than in the quenched theory, in agreement with our earlier result at $T = 0$ [12]. We believe that the introduction of dynamical fermions causes an attraction between monopoles and antimonopoles, which naturally leads to an increase in the monopole density. A similar mechanism has been observed in the case of instantons and anti-instantons [51]. Both mechanisms are, of course, related, because (anti-)instantons are intimately connected with monopoles [52].

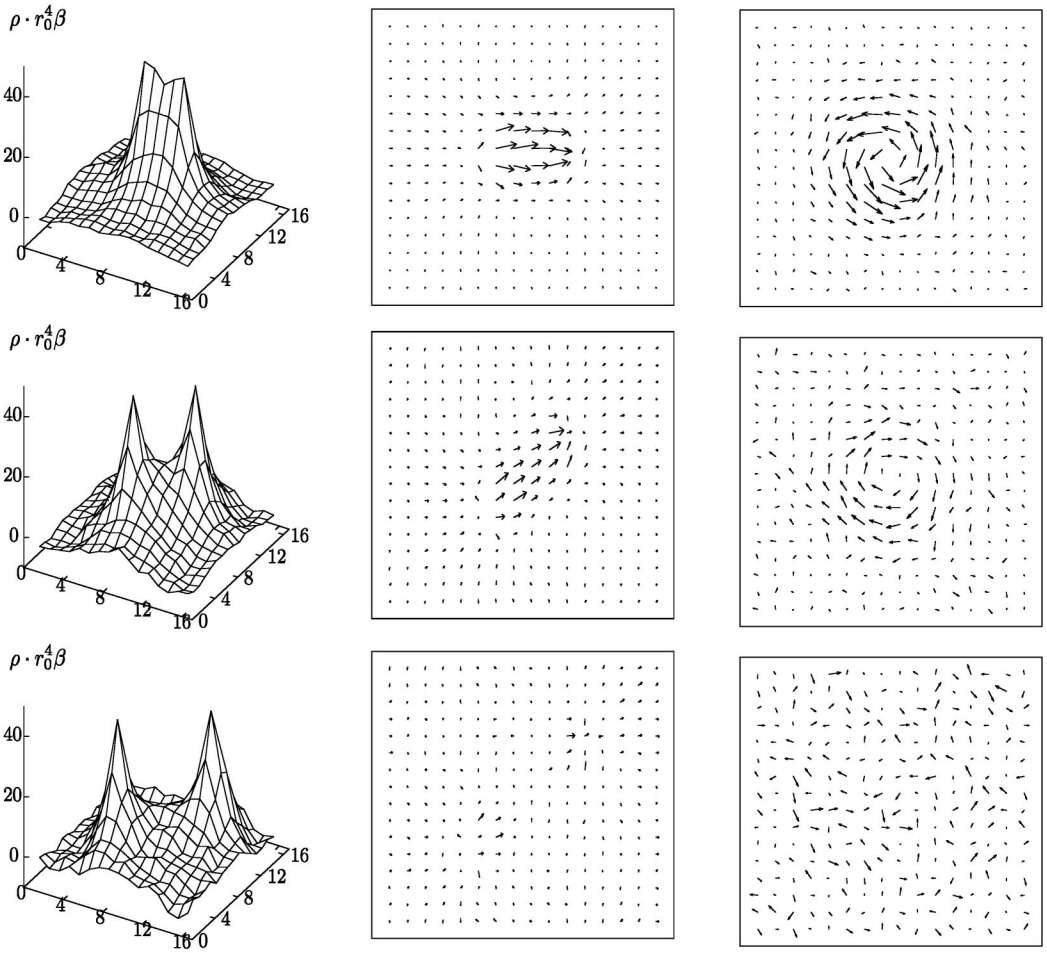


FIG. 20. The monopole part of the action density (a), the monopole part of the color electric field (b) and the solenoidal monopole current in the plane perpendicular to the flux tube (c) at $T/T_c = 0.979$ and distances (from top to bottom) 0.5, 0.8 and 1.3 fm.

Near the finite temperature transition we expect the monopoles to gradually become static as the temperature becomes high. This can be monitored by the asymmetry of the density of spatial and temporal monopole currents [28,53]:

$$\eta = \frac{\rho_t - \rho_s}{\rho_t + \rho_s}, \tag{43}$$

where $\rho_t(\rho_s)$ is the density of the temporal (spatial) monopole currents,

$$\rho_t = \frac{1}{3N_t N_s^3}\left\langle \sum_{i=1}^{3}\sum_{s} |k_i(^*s, 4)| \right\rangle,$$
$$\rho_s = \frac{1}{9N_t N_s^3}\left\langle \sum_{i=1}^{3}\sum_{s}\sum_{\mu=1}^{3} |k_i(^*s, \mu)| \right\rangle. \tag{44}$$

If all currents are timelike, then this quantity is unity, while in the case of an isotropic distribution it is zero. In Fig. 22 we plot the asymmetry $\eta$ as a function of temperature. We compare the result with the predictions of the quenched theory. It is found that $\eta$ is zero in the confined phase and nonzero in the deconfined phase. In the deconfinement phase the value of $\eta$ is about 5 times smaller in full QCD compared to the quenched theory. A reason for this

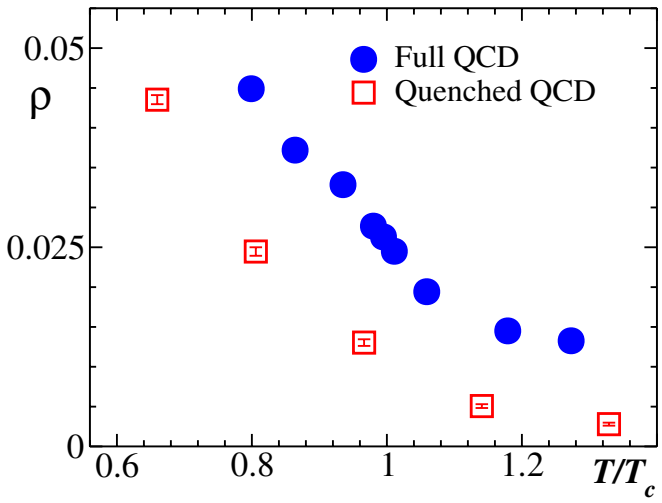


FIG. 21 (color online). The monopole density as a function of temperature.

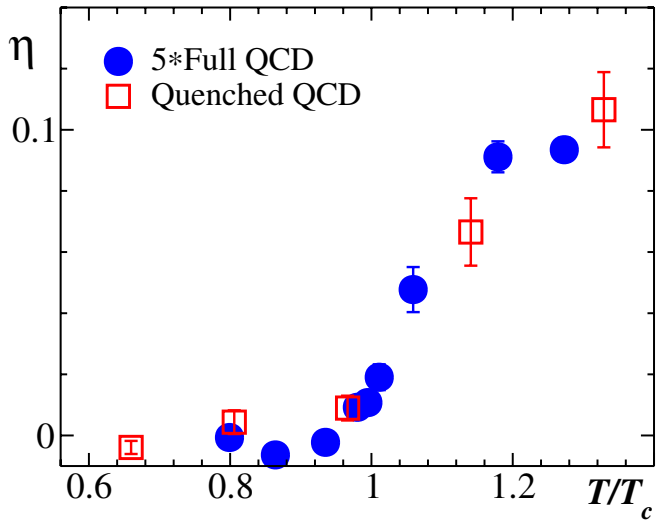


FIG. 22 (color online). The asymmetry of the monopole density as a function of temperature.

may be rooted in a different nature of the transition which is of the first order phase in the quenched case while in full QCD one observes a smooth crossover.

## VI. CONCLUSIONS

We have studied QCD with two flavors of dynamical quarks at finite temperature on a $16^3 8$ lattice. At the phase transition the lattice spacing is $a \approx 0.12$ fm. We employed nonperturbatively improved Wilson fermions, so that we may expect finite cutoff effects to be small.

To determine the parameters of the transition, notably the transition temperature and the string tension, and to shed light on the dynamics of the transition, it helped to resort to Abelian variables in the maximally Abelian gauge.

We observed string breaking in Polyakov loop correlators. This is a level crossing phenomenon. Accordingly, we fitted the correlator by a two-state ansatz, consisting of a string state and a two-meson state. We found good agreement of this ansatz with our numerical data for $T \lesssim T_c$, while we could rule out previously proposed single-state correlation functions. The string breaking distance was found to be $r_{\mathrm{sb}} \approx 1$ fm at $T/T_c \approx 0.8$, our lowest temperature. String breaking is also clearly visible in the action density, the color electric field distribution and the solenoidal monopole current around the static sources.

To make contact with the chiral and continuum limit, we need to make simulations at other $\beta$'s and larger $N_t$. Work on $16^3 8$ lattices at $\beta = 5.25$ and on $24^3 10$ lattices at $\beta = 5.2$ is in progress. Preliminary results have been presented in [54].

## ACKNOWLEDGMENTS

We like to thank Alan Irving and Dirk Pleiter for assistance. The calculations have been performed on the Hitachi SR8000 at KEK Tsukuba and on the MVS 1000M at Moscow. We like to thank the staff of the Moscow Joint Supercomputer Center, especially A. V. Zabrodin, for their support. We furthermore thank Ph. De Forcrand, V. Mitrjushkin and M. Müller-Preussker for useful discussions. This work is partially supported by Grants No. INTAS-00-00111, No. RFBR 02-02-17308, No. RFBR 04-02-16079, No. RFBR-DFG 03-02-04016, No. RFBR 03-02-16941, No. DFG-RFBR 436RUS113/739/0. Support was also received from CRDF RPI-2364-MO-02. M. Ch. is supported by JSPS P01023. V. B. acknowledges support from JSPS RC30126103. T. S. is supported by JSPS Grant-in-Aid for Scientific Research on Priority Areas 13135210 and 15340073.

[1] F. Karsch, E. Laermann, and A. Peikert, Nucl. Phys. **B605**, 579 (2001).
[2] A. Ali Khan *et al.* (CP-PACS Collaboration), Phys. Rev. D **63**, 034502 (2001).
[3] B. Bolder *et al.*, Phys. Rev. D **63**, 074504 (2001).
[4] F. Karsch, M. T. Mehr, and H. Satz, Z. Phys. C **37**, 617 (1988).
[5] G. 't Hooft, Nucl. Phys. **B190**, 455 (1981).
[6] A. S. Kronfeld, M. L. Laursen, G. Schierholz, and U.-J. Wiese, Phys. Lett. B **198**, 516 (1987).
[7] A. S. Kronfeld, G. Schierholz, and U.-J. Wiese, Nucl. Phys. **B293**, 461 (1987).
[8] H. Shiba and T. Suzuki, Phys. Lett. B **351**, 519 (1995); M. N. Chernodub, M. I. Polikarpov, and A. I. Veselov, Phys. Lett. B **399**, 267 (1997); A. Di Giacomo and G. Paffuti, Phys. Rev. D **56**, 6816 (1997).
[9] G. 't Hooft, in *High Energy Physics: Proceedings of the EPS International Conference, Palermo, 1975*, edited by A. Zichichi (Editrice Compositori, Bologna, 1976); S. Mandelstam, Phys. Rep. **23**, 245 (1976).
[10] Z. F. Ezawa and A. Iwazaki, Phys. Rev. D **25**, 2681 (1982); T. Suzuki and I. Yotsuyanagi, Phys. Rev. D **42**, 4257 (1990).
[11] For a review, see M. N. Chernodub and M. I. Polikarpov, hep-th/9710205.
[12] V. G. Bornyakov *et al.*, Nucl. Phys. Proc. Suppl. **B106**, 634 (2002).
[13] V. G. Bornyakov *et al.*, Phys. Rev. D **70**, 074511 (2004).
[14] J. D. Stack, S. D. Neiman, and R. J. Wensley, Phys. Rev. D **50**, 3399 (1994).
[15] H. Shiba and T. Suzuki, Phys. Lett. B **333**, 461 (1994).

[16] G. S. Bali, V. G. Bornyakov, M. Muller-Preussker, and K. Schilling, Phys. Rev. D **54**, 2863 (1996).
[17] S. Ejiri, S. Kitahara, T. Suzuki, and K. Yasuta, Phys. Lett. B **400**, 163 (1997).
[18] Y. Mori *et al.*, Nucl. Phys. **A721**, C930 (2003); V. G. Bornyakov *et al.*, hep-lat/0301002; Nucl. Phys. Proc. Suppl. **B119**, 703 (2003).
[19] B. Sheikholeslami and R. Wohlert, Nucl. Phys. **B259**, 572 (1985).
[20] S. Booth *et al.* (QCDSF-UKQCD Collaboration), Phys. Lett. B **519**, 229 (2001); M. Göckeler *et al.* (QCDSF Collaboration), hep-ph/0409312.
[21] C. R. Allton *et al.* (UKQCD Collaboration), Phys. Rev. D **65**, 054502 (2002).
[22] R. G. Edwards and U. M. Heller, Phys. Lett. B **462**, 132 (1999).
[23] K. Jansen and R. Sommer (ALPHA Collaboration), Nucl. Phys. **B530**, 185 (1998).
[24] A. Ali Khan *et al.* (QCDSF Collaboration), Phys. Lett. B **564**, 235 (2003).
[25] U. Wolff (ALPHA Collaboration), Comput. Phys. Commun. **156**, 143 (2004).
[26] A. Hasenfratz and F. Knechtli, Phys. Rev. D **64**, 034504 (2001).
[27] V. G. Bornyakov, D. A. Komarov, and M. I. Polikarpov, Phys. Lett. B **497**, 151 (2001).
[28] F. Brandstater, U.-J. Wiese, and G. Schierholz, Phys. Lett. B **272**, 319 (1991).
[29] T. A. DeGrand and D. Toussaint, Phys. Rev. D **22**, 2478 (1980).
[30] J. Smit and A. van der Sijs, Nucl. Phys. **B355**, 603 (1991).
[31] T. Suzuki, S. Ilyar, Y. Matsubara, T. Okude, and K. Yotsuji, Phys. Lett. B **347**, 375 (1995); **351**, 603(E) (1995).
[32] H. Satz, Nucl. Phys. **A681**, 3 (2001).
[33] C. W. Bernard *et al.* (MILC Collaboration), Phys. Rev. D **56**, 5584 (1997).
[34] S. Aoki *et al.* (CP-PACS Collaboration), Nucl. Phys. Proc. Suppl. **B73**, 216 (1999).
[35] H. Satz, hep-ph/0111265.
[36] F. Gliozzi and P. Provero, Nucl. Phys. **B556**, 76 (1999).
[37] T. Suzuki and M. N. Chernodub, Phys. Lett. B **563**, 183 (2003); hep-lat/0211026.
[38] S. Digal, P. Petreczky, and H. Satz, Phys. Lett. B **514**, 57 (2001).
[39] S. Kratochvila and P. de Forcrand, Nucl. Phys. **B671**, 103 (2003).
[40] C. DeTar, O. Kaczmarek, F. Karsch, and E. Laermann, Phys. Rev. D **59**, 031501 (1999).
[41] O. Jahn and O. Philipsen, Phys. Rev. D **70**, 074504 (2004).
[42] M. Lüscher and P. Weisz, J. High Energy Phys. 07 (2002) 049.
[43] M. Gao, Phys. Rev. D **40**, 2708 (1989); see also Ph. de Forcrand, G. Schierholz, H. Schneider, and M. Teper, Phys. Lett. B **160**, 137 (1985).
[44] G. S. Bali *et al.* (TXL Collaboration), Phys. Rev. D **62**, 054503 (2000).
[45] A. Hasenfratz, R. Hoffmann, and F. Knechtli, Nucl. Phys. Proc. Suppl. **B106**, 418 (2002).
[46] O. Kaczmarek, F. Karsch, E. Laermann, and M. Lutgemeier, Phys. Rev. D **62**, 034021 (2000).
[47] R. D. Pisarski and O. Alvarez, Phys. Rev. D **26**, 3735 (1982).
[48] C. Y. Wong, Phys. Rev. C **65**, 034902 (2002).
[49] G. S. Bali, K. Schilling, and C. Schlichter, Phys. Rev. D **51**, 5165 (1995); R. W. Haymaker, V. Singh, Y.-C. Peng, and J. Wosiek, Phys. Rev. D **53**, 389 (1996).
[50] V. Singh, D. A. Browne, and R. W. Haymaker, Phys. Lett. B **306**, 115 (1993);M. Zach, M. Faber, W. Kainz, and P. Skala, Phys. Lett. B **358**, 325 (1995); G. S. Bali, C. Schlichter, and K. Schilling, Prog. Theor. Phys. Suppl. **131**, 645 (1998).
[51] A. Hasenfratz, Phys. Lett. B **476**, 188 (2000).
[52] A. Hart and M. Teper, Phys. Lett. B **371**, 261 (1996); V. G. Bornyakov and G. Schierholz, Phys. Lett. B **384**, 190 (1996); M. N. Chernodub and F. V. Gubarev, JETP Lett. **62**, 100 (1995).
[53] S. Hioki, S. Kitahara, S. Kiura, Y. Matsubara, O. Miyamura, S. Ohno, and T. Suzuki, Phys. Lett. B **272**, 326 (1991); **281**, 416(E) (1992).
[54] Y. Nakamura *et al.*, Nucl. Phys. Proc. Suppl. **B129**, 733 (2004).